ACS NANO

www.acsnano.org

ARTICLE

Direct DNA Methylation Profiling with an Electric Biosensor

Deependra Kumar Ban,◇ Yushuang Liu,◇ Zejun Wang,◇ Srinivasan Ramachandran,◇ Nirjhar Sarkar, Ze Shi, Wenhan Liu, Abhijith G. Karkisaval, Erick Martinez-Loran, Feng Zhang, Gennadi Glinsky,* Prabhakar R. Bandaru,* Chunhai Fan,* and Ratnesh Lal*

Cite This: *ACS Nano* 2020, 14, 6743–6751

Read Online

ACCESS | Metrics & More | Article Recommendations | Supporting Information

ABSTRACT: DNA methylation is one of the principal epigenetic mechanisms that control gene expression in humans, and its profiling provides critical information about health and disease. Current profiling methods require chemical modification of bases followed by sequencing, which is expensive and time-consuming. Here, we report a direct and rapid determination of DNA methylation using an electric biosensor. The device consists of a DNA-tweezer probe integrated on a graphene field-effect transistor for label-free, highly sensitive, and specific methylation profiling. The device performance was evaluated with a target DNA that harbors a sequence of the methylguanine-DNA methyltransferase, a promoter of glioblastoma multiforme, a lethal brain tumor. The results show that we successfully profiled the methylated and nonmethylated forms at picomolar concentrations. Further, fluorescence kinetics and molecular dynamics simulations revealed that the position of the methylation site(s), their proximity, and accessibility to the toe-hold region of the tweezer probe are the primary determinants of the device performance.

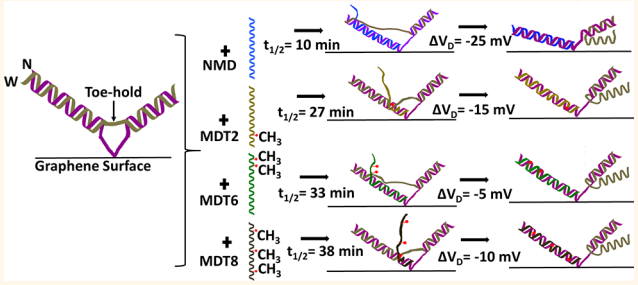

KEYWORDS: *DNA methylation, methylation profiling graphene field-effect transistor, DNA tweezers, Dirac voltage*

Among the epigenetic regulatory mechanisms, cytosine methylation is a major, long-term, and relatively stable gene alteration causing inheritable traits.[1,2] DNA methylation is implicated[3,4] in the normal development of brain, learning, aging, as well as in the pathogenesis of atherosclerosis, cancer, and others. Consequently, accurate methylation profiling is increasingly recognized as an important determinant in genetic screening for disease predisposition and predicting individual response to treatment. Current methylation profiling techniques rely on chemical modification of DNA bases[5] (*e.g.*, oxidation,[6] bisulfite conversion,[7] ferro-ferricyanide redox coupling,[8] methylation-specific digestion,[6] antibody binding[9]), thus limited by their chemical or enzymatic efficiency. Optical, electrochemical, and electronic biosensors for detecting DNA methylation also have several drawbacks[10] as they still depend on chemical modification of DNA,[11] antibody conjugation,[12] protein activity,[13−17] and chemical labeling.[18,19] Moreover, such techniques are often performed along with sequencing methods that require expensive reagents, sophisticated instrumentation, and highly trained personnel and are time-consuming.[20,21] Profiling by nanopore depends on methylation-specific ion current and complex data analysis, such as hidden Markov models (HMMs),[22,23] which require a large number of DNA profiles to reduce the error rate.[24] In summary, in the current state of the art, there does not seem to be a reliable DNA methylation profiling technology that does not require base modification(s).

Here we report the development of a direct, label-free, lab-on-chip device that enables sensitive and specific DNA methylation profiling (DMP). The device consists of a DNA tweezer probe (DTP),[25] integrated with a graphene field-effect transistor (GFET),[26] which discriminates methylated *vs* nonmethylated DNA targets at picomolar (pM) concentrations. The underlying sensing modalities are based on a strand-specific displacement reaction followed by sensitive surface charge detection. An electronic readout, through monitoring the voltage shifts, yields insight into the configurational modifications of target/DTP complexes and information on the methylation profiling.

Received: December 23, 2019
Accepted: May 14, 2020
Published: May 14, 2020

https://dx.doi.org/10.1021/acsnano.9b10085
ACS Nano 2020, 14, 6743–6751

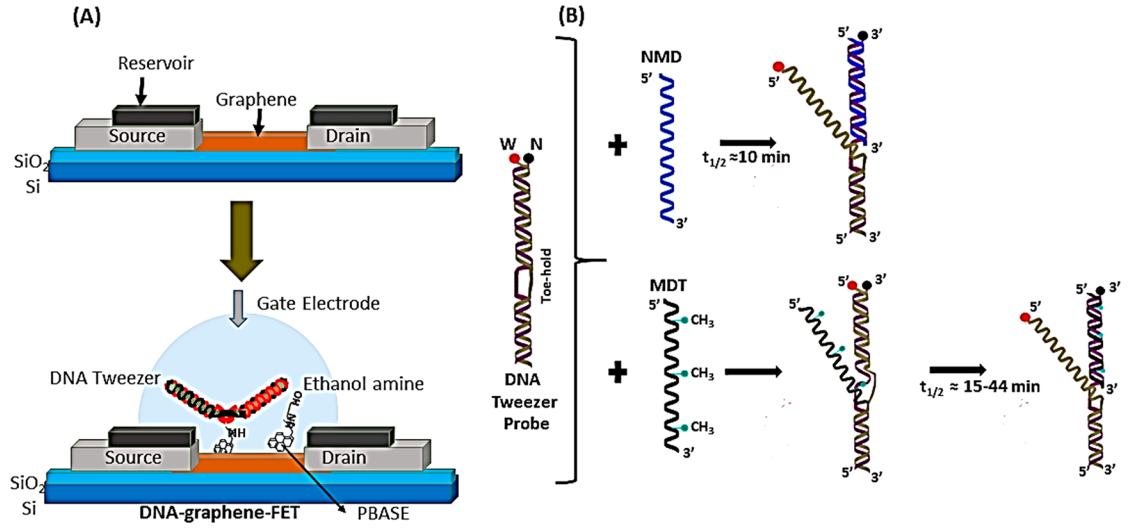

Figure 1. (A) Schematic of the DNA tweezer probe conjugation to the GFET, indicating the source and drain electrodes. Silicone paste used to insulate the electrodes and to create an electrolyte reservoir in the middle. (B) Schematic of strand displacement by NMD (top) and MDT (bottom). The W and N in the probe refer to the weak and the normal strands, respectively. Time to reach half of the fluorescence maxima ($t_{1/2}$, in minutes) was used as a metric for the probe-target interaction. A longer $t_{1/2}$ was observed for MDT compared to the NMD.

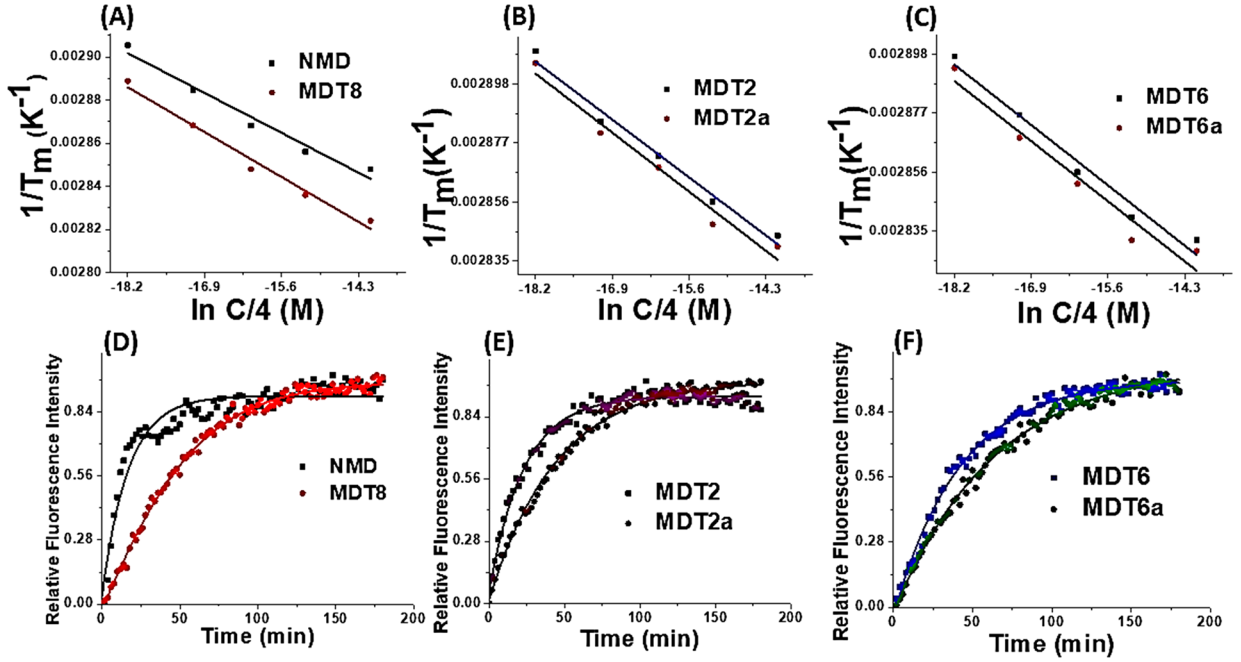

Figure 2. Concentration-dependent melting temperature analysis: (A) NMD and MDT8; (B) MDT2 and MDT2a; and (C) MDT6 and MDT6a. Kinetics of strand displacement and target hybridization: (D) NMD and MDT8; (E) MDT2, and MDT2a; and (F) MDT6 and MDT6a.

We first discuss the principle of strand displacement reaction in the DTP followed by the methylated DNA targets (MDT) used in this study. Describe the targets through melting temperature (T_m) and rate kinetics analyses. We then describe the direct label-free profiling of nonmethylated DNA (NMD) and MDT as well as between different [MDT]n (n is the number of methyl cytosines) with a GFET sensor. Finally, using molecular dynamics (MD) simulations, we provide insights about the mechanics of the target−probe interactions on the surface, which enable a better understanding of the process and develop more sensitive GFET devices in the future.

RESULTS AND DISCUSSION

DTP-GFET Sensor Preparation. A graphene-FET (GFET) was configured by transferring a ∼2 mm × 2 mm graphene film on to a silicon substrate. Silver epoxy was applied on either side of the graphene to act as source and drain electrode, and silicone paste was applied to insulate the electrodes and create a reaction well over the graphene, as shown in Figure 1A. A simple and more effective electrolyte gating method was utilized with reduced voltage compared to the back-gate approach.[27,28] The DTP backbone was functionalized with an amine group and immobilized on the graphene surface. The DTP is used to drive strand-specific displacement,

https://dx.doi.org/10.1021/acsnano.9b10085
ACS Nano 2020, 14, 6743−6751

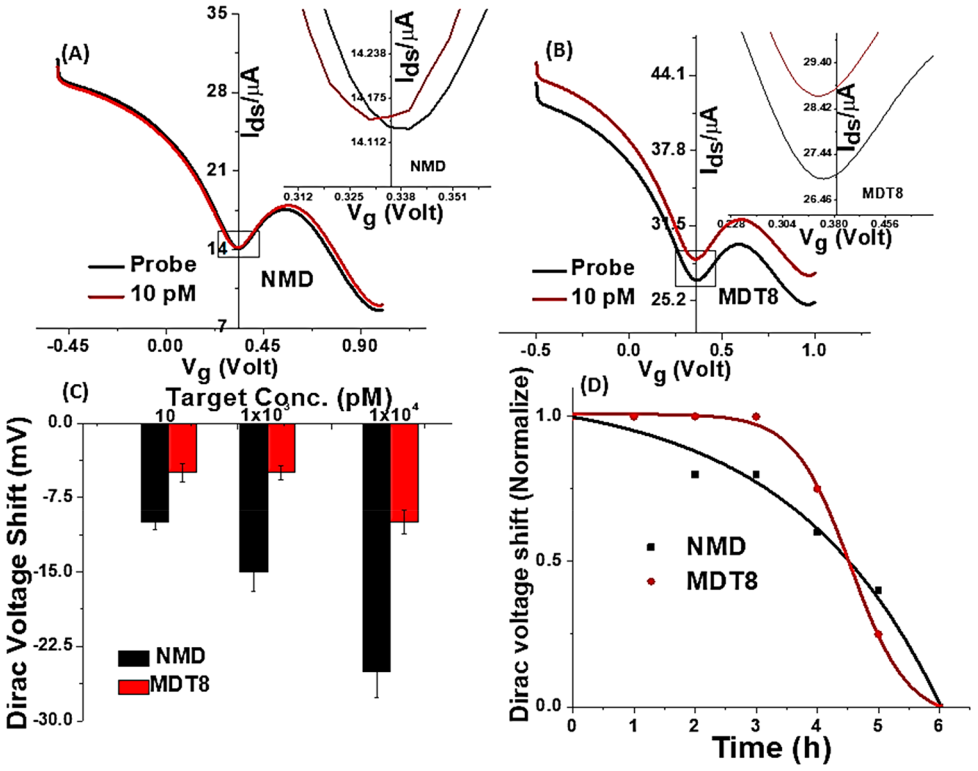

Figure 3. Direct, label-free DNA methylation profiling with GFET sensor. Concentration-dependent discrimination of methylated targets by Dirac voltage (V_D) shift measurements for (A) NMD and (B) MDT8. The insets depict the regions close to the V_D minimum. (C) Concentration-dependent V_D shift data for NMD and MDT8 (n = 3; $P \leq 0.05$). (D) The time-dependent V_D shift was analyzed at a 1 h interval up to 6 h for NMD and MDT.

and detection of NMD and [MDT]n (Figure 1B), and the GFET detects the charge modulation associated with strand displacement. The DTP sequence used in the experiments, indicating the weak (W), normal (N), and amine modified (N) are listed in Table S1, and the NMD and [MDT]n targets and configurations used in the experiments are listed in Table S2 (Supporting Information).

Probe−Target Interaction Energy Drives Strand Displacement/Hybridization. During the strand displacement reaction (Figure 1B), the incumbent W strand (weak strand) in the DTP is displaced by the invader strand (target strand) due to its higher affinity to the normal (N) strand. A toe-hold-mediated strand displacement reaction is thermodynamically favored and modifies the DTP.[29] Melting temperature (T_m) analysis provided insights into the energetics that drives the target−DTP interaction. T_m of the DTP sensing part (first 25 nucleotides from 5′ end of N and the corresponding bases on 3′ end of W, NW25) at 3 μM was found to be ∼67.7 °C. Variation of T_m as a function of DNA concentration plotted as $1/T_m$ (K^{-1}) *vs* ln (C/4) M (Figure 2A−C) shows a higher thermal stability of target−probe complex compared to NW25. T_m for all tested targets (at 3 μM) was 10−13 °C higher compared to NW25 (Figures 2A−C; Table S3 Supporting Information), while T_m among the targets (NMD/[MDT]n) are relatively small (0.5−3 °C).

Local Nearest-Neighbor Energetics and Accessibility Factors Determine Target Discrimination. .Thermal analysis showed that T_m among the targets is only slightly higher (0.5−3 °C) than NW25, suggesting the strand displacement is thermodynamically less favorable. However, strand displacement is primarily driven by the nearest-neighbor energetics between the base pairs and their accessibility to initiate the reaction at the toe-hold region.

We wondered whether real-time monitoring of strand displacement kinetics would provide any insights. From the fluorescence kinetics plots, the time to reach half of the maximal fluorescence ($t_{1/2}$) was determined (Figures 2D−F; Figure S2 and Table S4 in the Supporting Information). NMD targets rapidly displaced W strands with a $t_{1/2}$ ∼ 10.5 min. DNA methylation significantly slowed down the kinetics (Figure 2D). Also, for a given number of methylations per target, their position within the sequence, mainly, with respect to the toe-hold region, determines the kinetics. If the methylation site is located more toward the toe-hold region (MDT2a and MDT2b, $t_{1/2}$ = 32.7 and 27.8 min, respectively), the reaction was much slower compared to the methylation sites away from the toe-hold/toward the 5′ end (MDT2, $t_{1/2}$ ∼ 15.5 min, Figure 2E). For example, targets with six methylation bases located close to the toe-hold region slowed down the kinetics (MDT6a and MDT6b, $t_{1/2}$ ∼ 44.7 and 33.1 min, respectively) compared to targets with the same number of methylation sites, but located away from toe-hold region (MDT6, $t_{1/2}$ ∼ 30.5 min, Figure 2F).

The fluorescence kinetics results suggest that steric hindrance from methyl groups affects the structure and accessibility of DNA bases for displacement/hybridization. Also, methylated cytosines (mC) at the 3′ end (toe-hold region) resulted in the longest $t_{1/2}$ due to steric hindrance and local energy barriers. Additionally, physicochemical changes such as an increased DNA persistence length[30] (due to the methylation)[31] and associated accessibility slow down normal base-pairing kinetics.[32] Under these circumstances, the nearest-

https://dx.doi.org/10.1021/acsnano.9b10085
ACS Nano 2020, 14, 6743−6751

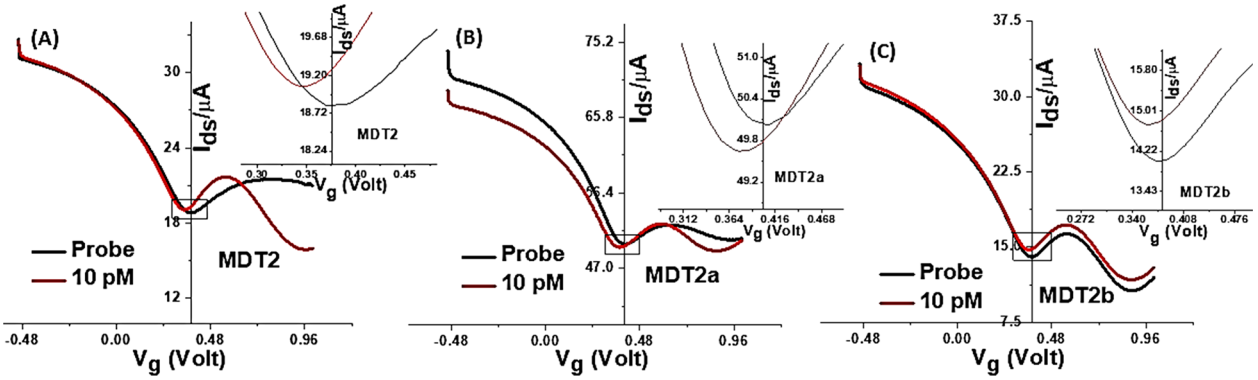

Figure 4. Comparison of the MDT*n* in three different GFETs. (A) MDT2, (B) MDT2a, and (C) MDT2b all have 2 mC groups at different locations in the target strand (Table S2, Supporting Information). V_D shifts to increasing positive voltages from MDT2 → MDT2a → MDT2b.

neighbor energetics of adjoining base pairs determines the overall kinetics. The spatial location, as well as the number of mC, plays a vital role in the strand displacement kinetics. A comprehensive understanding of these factors warrants a detailed study that is beyond the scope of this current work. However, a key finding is that for unbiased discrimination of an MDT, the methylation sites should be closer to the toe-hold region.

Methylated bases close to the toe-hold region could strongly influence the charge screening from the electrolytes and the substrate. The sensitivity relevant to a specific MDT moiety was sought to monitor through field-effect transistors (FET), which is exquisitely sensitive to charge-related modulations.

Label-Free Direct Methylation Profiling by Graphene FET Device. The estimated physical length of 51 bp DTP is ∼17 nm, it is longer than the Debye length (λ_D of ∼1.7 nm at 30 mM buffer), yet less than the typical DNA persistence length of 39 nm.[33] Methylation increases the persistence length of DNA,[30] which may affect its orientation with the substrate that may also influence the charge distribution close to the surface where the DTP is anchored to the graphene surface. It is expected that a GFET could monitor the DNA methylation associated changes, and specific MDT moieties, more sensitively than kinetic studies. Another advantage is that such changes could be quickly monitored through electrical current or potential variations in the FET.

An advantage of graphene is that the density of states (DOS) is theoretically zero at particular energy and equivalent voltage,[34] correspondings to the Dirac point. Consequently, any modulation around the Dirac point voltage (V_D), say from charge variations, would be subject to significant amplification. However, in practice, there could be a finite DOS at the Dirac point, due to impurities. For instance, ambient oxygen (also from the underlying silicon oxide) would induce p-type charge variations in the graphene and shift the V_D of a nominal graphene sheet to a positive value. However, the negative charge in the DNA[35] may compensate the V_D shift. Moreover, the inductive effect of the methyl groups[36] on the mC would further modulate the V_D. It is known that DNA hybridization causes a negative shift in V_D; therefore, any change in DNA hybridization can be detected in terms of V_D shift.[37] The principle of our GFET sensor is based on the relative charge modulation on the graphene surface by displacement of the weak strand by target DNA and its hybridization-mediated structural changes in the probe. We utilized this principle to detect DNA methylation-mediated changes on the GFET sensor.

Different concentrations of NMD changed V_D proportionately from −10 to −25 mV, which signifies the negative doping effect through NMD hybridization with DTP and adsorption on GFET (Figure 3A,C). The positive and negative slopes of the $I_{ds}-V_g$ curves (in addition to multiple minima/related Dirac points) are due to a charge transfer between the graphene and the metal electrodes.[38] This is also attributed to different doping levels along the graphene, away or near the contacts, for instance.[39] There is always a net current at the Dirac point voltage (V_D), which arises from capacitance contributions (from the double layer at the electrolyte−graphene interface, the quantum capacitance of the graphene, *etc.*), and a voltage scan rate (dV/dt) yields a conductance of the order of ∼1 nS.

Moreover, typical hysteresis in the sweeps is below 10 mV, less than the observed V_D shifts in the experiments. The hysteresis is systematic, typically in the same direction as the voltage scan, that is, right (/left) shift to increasing (/decreasing) voltages and does not add to the discussion related to the discrimination between the NMD and MDT moieties.

Generally, the GFET sensor response was reproducible over three cycles of testing, in any device. The error bars were determined using the standard deviation of the response over the testing cycles, assuming random errors. Moreover, the "probe", in the absence of a target NMD/MDT, served as an internal reference to which the Dirac point voltage shift/s were measured. However, when different GFET devices were used, the electrical current differed by a factor of 2−3. A similar experiment was performed with methylated DNA targets, and the results show that GFET can discriminate MDT8 at a 10 pM to 10 nM range of concentrations (V_D: −5 to −10 mV, Figure 3B,C). The delayed ΔV_D kinetics further confirms methylation-mediated steric hindrance in strand displacement reaction on the GFET surface (Figure 3D).

Label-free discrimination of NMD and MDT8 further warrants a detailed analysis of the role of methylation sites and their number on the V_D shift. It will further broaden the applicability of the GFET for discriminating against different MDT*n*. We measured the MDT2*n* strands in three different FETs, as indicated in Figure 4. We compared MDT2, MDT2a, and MDT2b (which all have two mC groups at different locations along the DNA chain, see Table S2 in Supporting Information) with respect to the location of the V_D. The V_D

https://dx.doi.org/10.1021/acsnano.9b10085
ACS Nano 2020, 14, 6743−6751

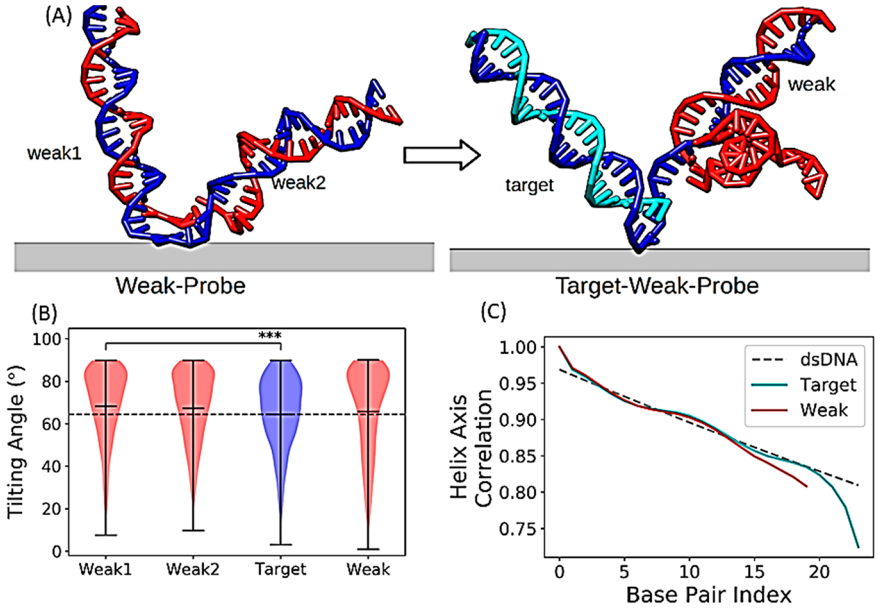

Figure 5. (A) Snapshots of a simulation showing the dynamics of DNA probe-target interaction on the surface. (B) Violin plot of distribution of the tilting angle between the duplex domains and the graphene surface. The width of each stick indicates the probability density of each of the angles. The means of two weak duplex domains without target hybridization [Weak1 and Weak2, in (A), left side] are found to be 68.37° and 67.34°, respectively. With the hybridized target, the target and weak duplex domains [(A), right side] are 64.44° and 65.71° ($p \leq 0.001$), respectively. (C) The correlation of the helix axis for the two duplex domains and free dsDNA after the target strand is added to the system.

shifts for MDT2b (near toe-hold region) and MDT2 (away from toe-hold) are −10 to −15 mV and −30 to −35 mV, respectively.

V_D shifts to increasingly positive voltages from MDT2 → MDT2a → MDT2b, indicating the inductive effect of the methyl groups. Such charge modulation from the methyl groups would be further combined with the negative charge from the DTP complex. Hence, the V_D shifts are small and need to be carefully calibrated. While the I_{ds} for MDT2 (Figure 4A) and MDT2b (Figure 4C) are similar, the I_{ds} for MDT2a is higher by a factor of 2. The reason for this discrepancy is unclear. We believe that referencing the target curves to the "probe" can reduce such variation in the background current and related errors. In many of our experiments, the magnitude of I_{ds} decreases with increasing target concentrations (Figure S3, Supporting Information), which may be due to increased binding to the graphene surface.

A similar trend was observed for targets with six methylation sites (see target sequence in Table S2 in Supporting Information). The less shift in V_D of targets having a methylcytosine closer to toe-hold region might be due to target-DTP hybridization-mediated structural changes near the toe-hold region. Figure S4 (Supporting Information) indicates the time series evolution of the Dirac voltage and possible methylation-mediated delay in the V_D shift in the mC close to the toe-hold region. The influence of mC location is less apparent in the kinetics of MDT2 and MDT6 (Figure S4, Supporting Information). While it seems that MDT6 has a quicker change of ΔV_D compared to MDT2, it is difficult to rank their kinetics. For example, at 4 h, MDT6 is more responsive, but not at 2 h. It would be pertinent to investigate the possible mechanisms of this differential response of the probe−target complex on the graphene surface through computational simulation.

Molecular Dynamics Simulations of Target−Probe Interaction. For a better understanding of the mechanics of the target−probe interactions, which would enable insight into the choice and interpretation of the MDT*n* results, a coarse-grained model MD simulation was performed, with snapshots from the modeling indicated in Figure 5.

The free duplex DNA, shown in Figure 5A, is considered as a reference structure for the simulations. The root-mean-square displacement (RMSD) of the duplex domains indicate their rigidity with respect to the surface. The tilting angle between the DNA duplex and the surface before and after the target strand hybridization is shown in Figure 5B, indicating that the target addition leads to a decrease in the tilting angle and the probability distribution shifts more uniformly about the mean, indicating a greater flexibility and comparatively more significant perturbations at the end of the target strand duplex domain (toward toe-hold region). For the target strand duplex, the strand could only bend at the end of the domain, while for the weak strand duplex, the deformation can be accumulated at the single-strand, that is, at the toe-hold region, between the duplex and the base bond on the surface as indicated by the helix axis correlation in plot Figure 5C.

Consequently, with methylation in the target strand, which increases the persistence length,[31] deformation in the duplex will be smaller. The strands would have a lower propensity to stay in states that require sharp bending. The altered physiochemical property of the probe−target complex and its effect on strand displacement is reflected in the magnitude of the observed V_D shifts as well as in fluorescence kinetics.

The overall aim of this work was to probe local alterations along the DNA chain, as may occur in methylated DNA and its influence on strand displacement and hybridization. This was sought to be done based on the tweezer probe interactions by comparing nonmethylated against methylated DNA. Initial studies with respect to the variation in T_m values were unable to differentiate NMD and MDTs significantly, but indicated that toe-hold-mediated displacement was thermodynamically more stable compared to NW25. During the strand displace-

https://dx.doi.org/10.1021/acsnano.9b10085
ACS Nano 2020, 14, 6743−6751

ment reaction, the incumbent weak (W) strand, and the invading target strand, exchanges base pairs with the normal (N) strand by an unbiased random walk. Subsequently, toe-hold-mediated strand displacement reaction is thermodynamically favored and ultimately displaces the incumbent weak strand.[29] The results show that methylcytosine at the 3′ end (toe-hold region) takes the longest $t_{1/2}$ due to the energy barrier. Here, the steric hindrance at the beginning of the reaction with the methylated strand slows down the strand displacement rate. In addition, physicochemical changes such as an increase in the persistence length and electronic properties of DNA and associated accessibility factors may interfere with normal base-pairing kinetics.[32] Under these circumstances, the nearest-neighbor energetics determines base-pairing and its kinetics. The measured $t_{1/2}$ of each target DNA revealed that the position of mC, number, and nearest-neighbor interaction energies play a vital role in the strand displacement kinetics.

It can also be inferred that a higher melting temperature (T_m), a measure of interaction energy, between the active sites of DTP-targets reflects to some extent the strand displacement/hybridization reaction of methylated and nonmethylated targets. The inclusion of inosines and ssDNA (the toe-hold region) is a key strategy for the high-efficiency and specificity of DTP. The altered physicochemical property of the probe-target complex and its effect on strand displacement is reflected in the change of kinetics of fluorescence analysis.

Subsequent investigations with the GFET sensor differentiated methylated targets with excellent sensitivity even at pM concentrations when the methylation site(s) is/are located near the toe-hold region. Related investigations confirmed that the presence of the methyl group toward the toe-hold region also caused a time delay in strand displacement with a relatively larger $t_{1/2}$ and small Dirac point voltage shift (Figure 3A–C).

CONCLUSIONS

Our DTP-GFET-based methodology can address some of the critical bottlenecks in DNA methylation profiling, including direct label-free detection with relative simplicity, high sensitivity and specificity, and portability. Since epigenetic reprogramming happens at the early embryonic stage (around blastocyst) and in primordial germ cells, presently used techniques need large amounts of sample, which is not possible. Generally, traditional methods for methylation detection such as disulfide conversion,[40,41] enzymatic digestion,[42,43] antibody binding[44,45] are robust and relatively sensitive; however, they are severely limited by high cost and typical requirements such as large amounts of sample, multiple steps of preprocessing, *etc.* The proposed biosensor-based DNA methylation technology seeks to advance detection modalities through the development of a portable, sensitive biosensor while using a small amount of sample (see a comparison to extant methodologies[46−49] in Table S5 of the Supporting Information). The underlying principles are based on strand displacement reaction and subsequent differential structural configuration of NMD and MDT*n* on GFET and do not require traditional processing.

The proposed technique has the potential to detect intermediate states of DNA demethylation like 5-hydroxymethylcytosine and 5-formylcytosine that are difficult to detect with current techniques. The DTP-based target recognition could offer possibilities for detecting such state variations, with significant implications in epigenetics research.

METHODS

Fabrication of Graphene FET Chip. Several graphene FET were prepared by transferring a ∼2 × 2 mm size graphene film on to a silicon substrate. The film was annealed at 400 °C for 2 h under hydrogen/argon atmosphere to remove organic impurities. Silver epoxy was applied at two ends of the graphene to serve as the source and drain electrodes, and a silicone rubber was used to insulate source and drain electrodes as well as to create an aqueous reaction chamber for strand displacement reaction in the middle (Figure 1A).[25] The measurements were all done with a constant V_{ds} of ∼30 mV. The gate was applied to the electrolyte and regulated its potential (see Figure 1). Consequently, there was always an I_{ds}. Typical gate leakage was of the order of nA, and orders of magnitude were below the typical I_{ds}. The electrolyte gate voltage range (∼1 V in 30 mM buffer solution) used for V_g is in accord with previous electrolyte gating measurements on graphene.[27]

Design of DTP for Target Discrimination. A DTP of 51 bp long comprising a weak strand (W) and a normal strand (N) was designed. There is a nine base long noncomplementary region called a toe-hold present in the middle of the N strand that prevents hybridization with W and provides the point of attack (strand displacement/hybridization in tandem) for the target strand. Further, the W strand was engineered to have six inosines (I) substituted for guanine (between 1 and 21 base positions) that pairs weakly with cytosine, in N strand (Table S1 in Supporting Information). This substitution lowers NW interaction affinity and favors strand displacement by a target with a better affinity (higher interaction energy). The DTP backbone is functionalized with an amine group to immobilize on the graphene surface of the GFET.

For fluorescence detection of strand displacement, Texas red (TR) and black hole quencher (BHQ2) were tagged at the 5′ and 3′ ends of W and N strands, respectively. The DTP strands were suspended in Tris-HCl buffer supplemented with 2 mM MgCl2 (pH 7.4). The strands were annealed in a thermocycler, and target displacement kinetics was monitored by fluorescence (Ex/Em: 590/620 nm)[50] in a plate reader at RT (Tecan Infinite 200 M).

DTP Immobilization on GFET. 50 μL of pyrenebutyric acid *N*-hydroxysuccinimide ester (PBASE, 5 mM) was deposited on graphene and incubated at room temperature for 1 h followed by a rinse with DMF and DI water.[25,51] Amine-functionalized DTP (1 μM) (IDT, Inc.) was immobilized on the graphene surface through PBASE conjugation by incubating it for 2 h at room temperature. The unreacted PBASE was passivated with 50 μL ethanolamine (100 mM) and further rinsed with Tris buffer.

Methylated DNA Targets. A 25 nucleotide-long DNA sequence that shares 20 nucleotides of methyl guanine methyl transferase (MGMT) promotor in glioblastoma multiforme[52] was chosen as the target (IDT, Inc.). Strands having a different number of methylation sites and positions were designed (Table S2), for example, MDT2, MDT2a, and MDT2b contain two; MDT6, MDT6a, and MDT6b contains six; MDT8 contains eight methylcytosines, and non-methylated DNA (NMD) target used as a control strand (see Table S2 in Supporting Information for a catalog of all the tested samples and configurations).

Melting Temperature Characterization of DNA Tweezer Probe−Target interaction. The DTP-target (NMD and MDTs) interaction energies were characterized by melting temperature (T_m) analysis with SYBR green fluorescence in a thermocycler. The T_m value of active part of DTP and DNA target was determined by annealing N strand (full length 51 NT) with a target strand (25 NT). Similarly, T_m of DTP and W strand (25 NT from 5′ end) (NW25) was determined for comparison and predicted the likelihood of reaction possibilities. Different concentrations (50, 150, 400, 1000, and 3000 nM) of hybridized probe and target were melted in a thermocycler, and the results were plotted as the natural log of molar concentration (C) to the inverse of respective melting temperatures

https://dx.doi.org/10.1021/acsnano.9b10085
ACS Nano 2020, 14, 6743−6751

(T_m) (Figure 2A–C and Figure S1 in the Supporting Information).[20] All the T_m values reported at 3 μM of sample concentration as a mean ± standard deviation (SD) and n = 3 (as in Table S3 of the Supporting Information).

Fluorescence Analysis of DNA Strand Displacement Kinetics. Target hybridization with DTP was inferred through W strand displacement-mediated fluorescence. Ten nM of DTP was mixed with 1 μM of a target strand in a 100 μL volume. Displacement of W by a target leads to the separation of TR from the quencher BHQ giving rise to an increase in fluorescence. This time series evolution of fluorescence provides the kinetics of a strand displacement reaction (Figure 2D–F and Figure S2 in Supporting Information), and the data were collected at 1 min intervals for up to 3 h (time to reach stable fluorescence). Normalized data averaged from three independent experiments are reported as ($t_{1/2}$) the time to reach half of the stable fluorescence. The data were normalized using the following equation:

$$F = \frac{F_t - F_{min}}{F_{max} - F_{min}} \quad (1)$$

where F is the normalized fluorescence, F_t is the fluorescence at time (t), F_{min} is the fluorescence minima (background fluorescence at time t = 0), and F_{max} is the fluorescence maxima (stable fluorescence at the end of 3 h).

Target Hybridization on the GFET Sensor. The strand displacement reactions were carried out with targets (NMD and MDT) at different concentrations, ranging from 10 pM to 10 nM in 50 μL of reaction volume. The sample was localized within the sample reservoir on the GFET sensor and incubated for 6 h. The unbound targets were rinsed off with Tris buffer before making the measurements. A time series evolution of the Dirac voltage shift provides the kinetics of strand displacement reaction (Figure 3D), and the data were collected at 1 h intervals for up to 6 h (time to reach stable Dirac shift). The normalized Dirac voltage (V_D) shift ($\Delta V_D = \frac{V_t - V_F}{V_o - V_F}$), where V_t is the value of the V_D at a given time (t), V_o is the initial value of the V_D at the start of the experiment/recording, and V_F is the value of the V_D after 6 h. The reservoir was covered using a small lid to avoid evaporation of liquid for 6 h. The points were connected as a guide to the eye.

Electrical Measurements. Source–drain current (I_{ds}) was recorded as a function of applied gate voltage (V_g) in the range of −0.5 to 1.0 V. A silver wire immersed in the reaction chamber buffer (2 mM $MgCl_2$/30 mM Tris buffer) acted as a gate electrode. Drain–source current (I_{ds}) was measured at an assigned V_{ds}. The effect of different target concentrations on I–V characteristics was studied in terms of a shift in Dirac point voltage (ΔV_D) of GFET. All of the obtained results were reliable and reproducible, with respect to systematic error metrics.

MD Simulation of DTP–Target Interaction. The MD simulation was performed using a recently developed coarse-grained model, oxDNA.[29] We used probe sequences similar to the ones used in experiments but without inosine, as the standard force field corresponding to inosine is not available in oxDNA. For the simulation of the strand displacement reaction, target sequences similar to NMD were used. The main objective was to understand the spatial orientation of the duplex regions of DTP before and after hybridization with the target strand. As the exact changes introduced by methyl groups on the structure of dsDNA are not well-known, we set up our simulation from the perspective of geometry changes in the toe-hold region and its corresponding effects on angular change of duplex regions to the horizontal surface. For the equilibration of DTP before hybridization with the target, we intentionally created base mismatches in the toe-hold region, effectively making the toe-hold region single-stranded and flexible. Then, in order to simulate the hybridization aspect, the target sequence (NMD) without any mismatches in the toe-hold region was allowed to interact with DTP. The simulation time step was set at 15.15 fs in a 303 ns long simulation, and it was performed under constant temperature (300 K) with sequence dependency.[53] Distribution of orientation angles (DTP to the graphene surface) with and without the target was created by sampling 1000 snapshots through the course of the simulation and visualized through violin plots. The ion concentration was set to 150 mM Na^+, as oxDNA is not parametrized with Mg^{2+}. Since our main focus was understanding the geometrical aspects of dsDNA, we simplified the graphene side of the problem by approximating it with a repulsive potential wall. The base conjugation was modeled by a strong harmonic potential with force constant of 571 pN/nm^2. This strong restraint represents the strong binding affinity between modified DNA strands and graphene.

ASSOCIATED CONTENT

Supporting Information

The Supporting Information is available free of charge at https://pubs.acs.org/doi/10.1021/acsnano.9b10085.

Additional information about DNA sequences used in present work, fluorescence kinetics, melting temperature, and concentration-dependent Dirac voltage shift data. A table containing a comparison of different methylation detection techniques (PDF)

AUTHOR INFORMATION

Corresponding Authors

Gennadi Glinsky − *Institute of Engineering in Medicine, University of California San Diego, La Jolla, California 92093, United States*; Email: gglinskii@ucsd.edu

Prabhakar R. Bandaru − *Department of Mechanical and Aerospace Engineering and Materials Science and Engineering, University of California San Diego, La Jolla, California 92093, United States; Department of Nanoengineering, University of California, San Diego, La Jolla, California 92093, United States*; orcid.org/0000-0003-4497-9620; Email: pbandaru@ucsd.edu

Chunhai Fan − *CAS Key Laboratory of Interfacial Physics and Technology, Shanghai Institute of Applied Physics, Chinese Academy of Sciences, Shanghai 201800, China; School of Chemistry and Chemical Engineering, Frontiers Science Center for Transformative Molecules, and Institute of Molecular Medicine, Renji Hospital, School of Medicine, Shanghai Jiao Tong University, Shanghai 200240, China*; orcid.org/0000-0002-7171-7338; Email: fanchunhai@sjtu.edu.cn

Ratnesh Lal − *Department of Mechanical and Aerospace Engineering, Department of Bioengineering, Materials Science and Engineering, and Institute of Engineering in Medicine, University of California San Diego, La Jolla, California 92093, United States*; orcid.org/0000-0001-7256-126X; Email: rlal@ucsd.edu

Authors

Deependra Kumar Ban − *Department of Mechanical and Aerospace Engineering, University of California San Diego, La Jolla, California 92093, United States*

Yushuang Liu − *School of Life Science, Inner Mongolia Agricultural University, Hohhot 010018, China*

Zejun Wang − *CAS Key Laboratory of Interfacial Physics and Technology, Shanghai Institute of Applied Physics, Chinese Academy of Sciences, Shanghai 201800, China*

Srinivasan Ramachandran − *Department of Bioengineering, University of California San Diego, La Jolla, California 92093, United States*

Nirjhar Sarkar − *Materials Science and Engineering, University of California San Diego, La Jolla, California 92093, United States*

https://dx.doi.org/10.1021/acsnano.9b10085
ACS Nano 2020, 14, 6743–6751

Ze Shi − *Department of Mechanical and Aerospace Engineering, University of California San Diego, La Jolla, California 92093, United States*
Wenhan Liu − *CAS Key Laboratory of Interfacial Physics and Technology, Shanghai Institute of Applied Physics, Chinese Academy of Sciences, Shanghai 201800, China*
Abhijith G. Karkisaval − *Department of Mechanical and Aerospace Engineering, University of California San Diego, La Jolla, California 92093, United States*
Erick Martinez-Loran − *Department of Nanoengineering, University of California, San Diego, La Jolla, California 92093, United States;* orcid.org/0000-0003-3841-4981
Feng Zhang − *School of Life Science, Inner Mongolia Agricultural University, Hohhot 010018, China; State Key Laboratory of Respiratory Disease, Key Laboratory of Oral Medicine, Guangzhou Institute of Oral Disease, Stomatology Hospital, Department of Biomedical Engineering, School of Basic Medical Sciences, Guangzhou Medical University, Guangzhou 511436, China*

Complete contact information is available at: https://pubs.acs.org/10.1021/acsnano.9b10085

Author Contributions

◇These authors contributed equally to this work. D.K.B., P.R.B., G.G., and R.L. conceived the idea. D.K.B. designed the experiments. Y.L. and N.S. fabricated and characterized the GFET devices. Y.L., D.K.B., Z.W., and W.L. performed experiments. Simulation work was performed by Z.S. D.K.B. analyzed data. D.K.B. wrote a detailed explanation for all the results with P.R.B., S.R., and G.G. S.R., D.K.B., P.R.B., G.G., and R.L. wrote the paper. A.G.K. from RL group and E.M.L. from PB group provided important suggestions. All authors have approved the final version of the manuscript.

Notes

The authors declare no competing financial interest.

ACKNOWLEDGMENTS

The work is supported by grants from the National Institute of Aging 4R01AG028709-10 and departmental development funds from the Department of Mechanical and Aerospace Engineering, UCSD.

REFERENCES

(1) Moore, L. D.; Le, T.; Fan, G. DNA Methylation and Its Basic Function. *Neuropsychopharmacology* **2013**, *38*, 23−38.
(2) Jin, B.; Li, Y.; Robertson, K. D. DNA Methylation: Superior or Subordinate in the Epigenetic Hierarchy? *Genes Cancer* **2011**, *2*, 607−617.
(3) Rodenhiser, D.; Mann, M. Epigenetics and Human Disease: Translating Basic Biology into Clinical Applications. *CMAJ.* **2006**, *174*, 341.
(4) Klutstein, M.; Nejman, D.; Greenfield, R.; Cedar, H. DNA Methylation in Cancer and Aging. *Cancer Res.* **2016**, *76*, 3446.
(5) Shin, Y.; Perera, A. P.; Kee, J. S.; Song, J.; Fang, Q.; Lo, G.-Q.; Park, M. K. Label-Free Methylation Specific Sensor Based on Silicon Microring Resonators for Detection and Quantification of DNA Methylation Biomarkers in Bladder Cancer. *Sens. Actuators, B* **2013**, *177*, 404−411.
(6) Kato, D.; Goto, K.; Fujii, S.; Takatsu, A.; Hirono, S.; Niwa, O. Electrochemical DNA Methylation Detection for Enzymatically Digested CpG Oligonucleotides. *Anal. Chem.* **2011**, *83*, 7595−7599.
(7) Patel, V. B.; Preedy, V. R. *Handbook of Nutrition, Diet, and Epigenetics*; Springer Nature: Switzerland AG, 2019, pp 43−60.
(8) Zhu, B.; Booth, M. A.; Shepherd, P.; Sheppard, A.; Travas-Sejdic, J. Distinguishing Cytosine Methylation Using Electrochemical, Label-Free Detection of DNA Hybridization and Ds-Targets. *Biosens. Bioelectron.* **2015**, *64*, 74−80.
(9) Maki, W. C.; Mishra, N. N.; Cameron, E. G.; Filanoski, B.; Rastogi, S. K.; Maki, G. K. Nanowire-Transistor Based Ultra-Sensitive DNA Methylation Detection. *Biosens. Bioelectron.* **2008**, *23*, 780−787.
(10) Syedmoradi, L.; Esmaeili, F.; Norton, M. L. Towards DNA Methylation Detection Using Biosensors. *Analyst* **2016**, *141*, 5922−5943.
(11) Wang, P.; Wu, H.; Dai, Z.; Zou, X. Picomolar Level Profiling of the Methylation Status of the P53 Tumor Suppressor Gene by a Label-Free Electrochemical Biosensor. *Chem. Commun.* **2012**, *48*, 10754−10756.
(12) Hawk, R. M.; Armani, A. M. Label Free Detection of 5′hydroxymethylcytosine within CpG Islands Using Optical Sensors. *Biosens. Bioelectron.* **2015**, *65*, 198−203.
(13) Li, Y.; Luo, X.; Yan, Z.; Zheng, J.; Qi, H. A Label-Free Supersandwich Electrogenerated Chemiluminescence Method for the Detection of DNA Methylation and Assay of the Methyltransferase Activity. *Chem. Commun.* **2013**, *49*, 3869−3871.
(14) Pan, S.; Xu, J.; Shu, Y.; Wang, F.; Xia, W.; Ding, Q.; Xu, T.; Zhao, C.; Zhang, M.; Huang, P.; Lu, S. Double Recognition of Oligonucleotide and Protein in the Detection of DNA Methylation with Surface Plasmon Resonance Biosensors. *Biosens. Bioelectron.* **2010**, *26*, 850−853.
(15) Dai, Z.; Hu, X.; Wu, H.; Zou, X. A Label-Free Electrochemical Assay for Quantification of Gene-Specific Methylation in a Nucleic Acid Sequence. *Chem. Commun.* **2012**, *48*, 1769−1771.
(16) Wang, J.; Zhu, Z.; Ma, H. Label-Free Real-Time Detection of DNA Methylation Based on Quartz Crystal Microbalance Measurement. *Anal. Chem.* **2013**, *85*, 2096−2101.
(17) Zheng, X.-J.; Qiu, J.-D.; Zhang, L.; Wang, Z.-X.; Liang, R.-P. Label-Free Colorimetric Assay for DNA Methylation Based on Unmodified Au Nanorods as a Signal Sensing Probe Coupled with Enzyme-Linkage Reactions. *Chem. Commun.* **2013**, *49*, 3546−3548.
(18) Wu, Y.; Zhang, B.; Guo, L.-H. Label-Free and Selective Photoelectrochemical Detection of Chemical DNA Methylation Damage Using DNA Repair Enzymes. *Anal. Chem.* **2013**, *85*, 6908−6914.
(19) Li, J.; Yan, H.; Wang, K.; Tan, W.; Zhou, X. Hairpin Fluorescence DNA Probe for Real-Time Monitoring of DNA Methylation. *Anal. Chem.* **2007**, *79*, 1050−1056.
(20) You, Y.; Tataurov, A. V.; Owczarzy, R. Measuring Thermodynamic Details of DNA Hybridization Using Fluorescence. *Biopolymers* **2011**, *95*, 472−486.
(21) Song, Y.; Huang, Y.-Y.; Liu, X.; Zhang, X.; Ferrari, M.; Qin, L. Point-of-Care Technologies for Molecular Diagnostics Using a Drop of Blood. *Trends Biotechnol.* **2014**, *32*, 132−139.
(22) Simpson, J. T.; Workman, R. E.; Zuzarte, P. C.; David, M.; Dursi, L. J.; Timp, W. Detecting DNA Cytosine Methylation Using Nanopore Sequencing. *Nat. Methods* **2017**, *14*, 407.
(23) Rand, A. C.; Jain, M.; Eizenga, J. M.; Musselman-Brown, A.; Olsen, H. E.; Akeson, M.; Paten, B. Mapping DNA Methylation with High-Throughput Nanopore Sequencing. *Nat. Methods* **2017**, *14*, 411.
(24) Schreiber, J.; Wescoe, Z. L.; Abu-Shumays, R.; Vivian, J. T.; Baatar, B.; Karplus, K.; Akeson, M. Error Rates for Nanopore Discrimination among Cytosine, Methylcytosine, and Hydroxymethylcytosine along Individual DNA Strands. *Proc. Natl. Acad. Sci. U. S. A.* **2013**, *110*, 18910.
(25) Hwang, M. T.; Wang, Z.; Ping, J.; Ban, D. K.; Shiah, Z. C.; Antonschmidt, L.; Lee, J.; Liu, Y.; Karkisaval, A. G.; Johnson, A. T. C.; Fan, C.; Glinsky, G.; Lal, R. DNA Nanotweezers and Graphene Transistor Enable Label-Free Genotyping. *Adv. Mater.* **2018**, *30*, 1802440.
(26) Cai, B.; Wang, S.; Huang, L.; Ning, Y.; Zhang, Z.; Zhang, G.-J. Ultrasensitive Label-Free Detection of PNA−DNA Hybridization by Reduced Graphene Oxide Field-Effect Transistor Biosensor. *ACS Nano* **2014**, *8*, 2632−2638.

(27) Ohno, Y.; Maehashi, K.; Yamashiro, Y.; Matsumoto, K. Electrolyte-Gated Graphene Field-Effect Transistors for Detecting PH and Protein Adsorption. *Nano Lett.* **2009**, *9*, 3318−3322.
(28) Farmer, D. B.; Lin, Y.-M.; Avouris, P. Graphene Field-Effect Transistors with Self-Aligned Gates. *Appl. Phys. Lett.* **2010**, *97*, 013103.
(29) Srinivas, N.; Ouldridge, T. E.; Šulc, P.; Schaeffer, J. M.; Yurke, B.; Louis, A. A.; Doye, J. P.; Winfree, E. On the Biophysics and Kinetics of Toehold-Mediated DNA Strand Displacement. *Nucleic Acids Res.* **2013**, *41*, 10641−10658.
(30) Cassina, V.; Manghi, M.; Salerno, D.; Tempestini, A.; Iadarola, V.; Nardo, L.; Brioschi, S.; Mantegazza, F. Effects of Cytosine Methylation on DNA Morphology: An Atomic Force Microscopy Study. *Biochim. Biophys. Acta, Gen. Subj.* **2016**, *1860*, 1−7.
(31) Kaur, P.; Plochberger, B.; Costa, P.; Cope, S. M.; Vaiana, S. M.; Lindsay, S. Hydrophobicity of Methylated DNA as a Possible Mechanism for Gene Silencing. *Phys. Biol.* **2012**, *9*, 065001.
(32) Pérez, A.; Castellazzi, C. L.; Battistini, F.; Collinet, K.; Flores, O.; Deniz, O.; Ruiz, M. L.; Torrents, D.; Eritja, R.; Soler-López, M.; Orozco, M. Impact of Methylation on the Physical Properties of DNA. *Biophys. J.* **2012**, *102*, 2140−2148.
(33) Gross, P.; Laurens, N.; Oddershede, L. B.; Bockelmann, U.; Peterman, E. J. G.; Wuite, G. J. L. Quantifying How DNA Stretches, Melts and Changes Twist under Tension. *Nat. Phys.* **2011**, *7*, 731.
(34) Goerbig, M. Electronic Properties of Graphene in a Strong Magnetic Field. *Rev. Mod. Phys.* **2011**, *83*, 1193.
(35) Fan, R.; Karnik, R.; Yue, M.; Li, D.; Majumdar, A.; Yang, P. DNA Translocation in Inorganic Nanotubes. *Nano Lett.* **2005**, *5*, 1633−1637.
(36) Morrison, R.; Boyd, R. *Organic Chemistry*; Prentice Hall: Englewood Cliffs, NJ, 1992, Vol. 6, pp 519−521.
(37) Dong, X.; Shi, Y.; Huang, W.; Chen, P.; Li, L.-J. Electrical Detection of DNA Hybridization with Single-Base Specificity Using Transistors Based on CVD-Grown Graphene Sheets. *Adv. Mater.* **2010**, *22*, 1649−1653.
(38) Di Bartolomeo, A.; Giubileo, F.; Santandrea, S.; Romeo, F.; Citro, R.; Schroeder, T.; Lupina, G. Charge Transfer and Partial Pinning at the Contacts as the Origin of a Double Dip in the Transfer Characteristics of Graphene-Based Field-Effect Transistors. *Nanotechnology* **2011**, *22*, 275702.
(39) Barraza-Lopez, S.; Vanević, M.; Kindermann, M.; Chou, M.-Y. Effects of Metallic Contacts on Electron Transport through Graphene. *Phys. Rev. Lett.* **2010**, *104*, 076807.
(40) Herman, J. G.; Graff, J. R.; Myöhänen, S.; Nelkin, B. D.; Baylin, S. B. Methylation-Specific PCR: A Novel PCR Assay for Methylation Status of CpG Islands. *Proc. Natl. Acad. Sci. U. S. A.* **1996**, *93*, 9821−9826.
(41) Lister, R.; Pelizzola, M.; Dowen, R. H.; Hawkins, R. D.; Hon, G.; Tonti-Filippini, J.; Nery, J. R.; Lee, L.; Ye, Z.; Ngo, Q.-M.; Edsall, L.; Antosiewicz-Bourget, J.; Stewart, R.; Ruotti, V.; Millar, A. H.; Thomson, J. A.; Ren, B.; Ecker, J. R. Human DNA Methylomes at Base Resolution Show Widespread Epigenomic Differences. *Nature* **2009**, *462*, 315−322.
(42) Armstrong, K. M.; Bermingham, E. N.; Bassett, S. A.; Treloar, B. P.; Roy, N. C.; Barnett, M. P. Global DNA Methylation Measurement by HPLC Using Low Amounts of DNA. *Biotechnol. J.* **2011**, *6*, 113−117.
(43) Smiraglia, D. J.; Kazhiyur-Mannar, R.; Oakes, C. C.; Wu, Y.-Z.; Liang, P.; Ansari, T.; Su, J.; Rush, L. J.; Smith, L. T.; Yu, L.; Liu, C.; Dai, Z.; Chen, S.-S.; Wang, S.-H.; Costello, J.; Ioshikhes, I.; Dawson, D. W.; Hong, J. S.; Teitell, M. A.; Szafranek, A.; Camoriano, M.; et al. Restriction Landmark Genomic Scanning (RLGS) Spot Identification by Second Generation Virtual RLGS in Multiple Genomes with Multiple Enzyme Combinations. *BMC Genomics* **2007**, *8*, 446−446.
(44) Weber, M.; Davies, J. J.; Wittig, D.; Oakeley, E. J.; Haase, M.; Lam, W. L.; Schübeler, D. Chromosome-Wide and Promoter-Specific Analyses Identify Sites of Differential DNA Methylation in Normal and Transformed Human Cells. *Nat. Genet.* **2005**, *37*, 853−862.
(45) Brinkman, A. B.; Simmer, F.; Ma, K.; Kaan, A.; Zhu, J.; Stunnenberg, H. G. Whole-Genome DNA Methylation Profiling Using MethylCap-Seq. *Methods* **2010**, *52* (3), 232−236.
(46) Yin, H.; Sun, B.; Zhou, Y.; Wang, M.; Xu, Z.; Fu, Z.; Ai, S. A New Strategy for Methylated DNA Detection Based on Photoelectrochemical Immunosensor Using Bi_2S_3 Nanorods, Methyl Bonding Domain Protein and Anti-His Tag Antibody. *Biosens. Bioelectron.* **2014**, *51*, 103−108.
(47) Makowski, M. S.; Ivanisevic, A. Molecular Analysis of Blood with Micro-/Nanoscale Field-Effect-Transistor Biosensors. *Small* **2011**, *7*, 1863−1875.
(48) Zhang, G.-J.; Ning, Y. Silicon Nanowire Biosensor and Its Applications in Disease Diagnostics: A Review. *Anal. Chim. Acta* **2012**, *749*, 1−15.
(49) Green, N. S.; Norton, M. L. Interactions of DNA with Graphene and Sensing Applications of Graphene Field-Effect Transistor Devices: A Review. *Anal. Chim. Acta* **2015**, *853*, 127−142.
(50) Krepl, M.; Otyepka, M.; Banáš, P.; Šponer, J. Effect of Guanine to Inosine Substitution on Stability of Canonical DNA and RNA Duplexes: Molecular Dynamics Thermodynamics Integration Study. *J. Phys. Chem. B* **2013**, *117*, 1872−1879.
(51) Chen, R. J.; Zhang, Y.; Wang, D.; Dai, H. Noncovalent Sidewall Functionalization of Single-Walled Carbon Nanotubes for Protein Immobilization. *J. Am. Chem. Soc.* **2001**, *123*, 3838−3839.
(52) Nakagawachi, T.; Soejima, H.; Urano, T.; Zhao, W.; Higashimoto, K.; Satoh, Y.; Matsukura, S.; Kudo, S.; Kitajima, Y.; Harada, H.; et al. Silencing Effect of CpG Island Hypermethylation and Histone Modifications on O6-Methylguanine-DNA Methyltransferase (MGMT) Gene Expression in Human Cancer. *Oncogene* **2003**, *22*, 8835.
(53) Shi, Z.; Castro, C. E.; Arya, G. Conformational Dynamics of Mechanically Compliant DNA Nanostructures from Coarse-Grained Molecular Dynamics Simulations. *ACS Nano* **2017**, *11*, 4617−4630.

https://dx.doi.org/10.1021/acsnano.9b10085
ACS Nano 2020, 14, 6743−6751